

# Soft edge of hadron scattering and mini-jet models for the total and inelastic $pp$ cross sections at LHC and beyond

D. A. Fagundes\*

*Instituto de Física Teórica, UNESP, Rua Dr. Bento T. Ferraz,  
271, Bloco II, 01140-070, São Paulo - SP, Brazil*

A. Grau†

*Departamento de Física Teórica y del Cosmos,  
Universidad de Granada, 18071 Granada, Spain*

G. Pancheri‡

*INFN Frascati National Laboratories, Via E. Fermi 40, 00444, Italy*

Y. N. Srivastava§

*Physics Department, University of Perugia, 06123 Perugia, Italy*

O. Shekhovtsova¶

*Kharkov Institute of Physics and Technology 61108, Akademicheskaya,1, Kharkov, Ukraine  
Institute of Nuclear Physics PAN ul. Radzikowskiego 152 31-342 Krakow, Poland*

We show that the onset and rise of QCD mini-jets provide the dynamical mechanism behind the appearance of a *soft edge* in  $pp$  collisions around ISR energies and thus such a soft edge is *built in* our mini-jet model with soft gluon re-summation. Here the model is optimized for LHC at  $\sqrt{s} = 7, 8 \text{ TeV}$  and predictions made for higher LHC and cosmic ray energies. Further, we provide a phenomenological picture to discuss the breakup of the total cross section into its elastic, uncorrelated and correlated inelastic pieces in the framework of a one-channel eikonal function.

PACS numbers: 13.75.Cs, 13.85.-t

Keywords:  $pp$  total and inelastic collisions, Cosmic rays

---

\* dfagundes@ift.unesp.br

† igräu@ugr.es

‡ giulia.pancheri@lnf.infn.it

§ yogendra.srivastava@gmail.com

¶ olga.shekhovtsova@ifj.edu.pl

## I. INTRODUCTION

This paper has three main objectives: (i) to clarify the role played by QCD mini-jets in the high energy behavior of total cross sections in reference to recent observation about the onset of an energy invariant *soft edge* [1] in  $pp$  collisions, around CERN intersecting storage ring (ISR) energies; (ii) to provide an update of our model predictions at  $\sqrt{s} = 13$  and  $14$   $TeV$  (LHC13 and LHC14) for proton-proton scattering, both for total [2] and inelastic [3] cross sections and (iii) to apply our mini-jet model to the very high energy behavior that may be of utility for analyses of the particle production cross section in the realm of cosmic rays.

The paper is organized as follows. In Sec.(II), we begin by showing how the notion of mini-jets in its simplest formulation when augmented by asymptotic freedom leads easily to the appearance of a threshold in the total cross section around  $\sqrt{s} \simeq (10 \div 20)$   $GeV$ . Through the use of current Parton Density Functions (PDFs), we then show that the onset and the rise of the mini-jet cross section is behind the observation of the *soft edge*.

Having thus highlighted the role of the mini jet phenomenon in view of the recent observation of an *edge-like* structure [1, 4] occurring in hadronic collisions near  $\sqrt{s} \simeq (10 \div 20)$   $GeV$ , in Sec.(III), we provide a brief description of the model we have proposed quite a long time ago [5], which overcomes the main limitation of the mini-jet description, namely the violation of the Froissart bound, through soft gluon  $k_t$  re-summation. We take the opportunity to optimize our predictions for both LHC and higher energy  $pp$  data extracted from cosmic rays, and include recent results at  $\sqrt{s} = 7$  and  $8$   $TeV$ . We also indicate the uncertainty coming from different sets of PDFs entering the calculations.

In Sec.(IV), we apply our model to inelastic scattering at LHC and discuss the role played by mini-jets in non-diffractive scattering. A breakup of the inelastic cross section in terms of its correlated and uncorrelated parts and the extraction of the measured elastic cross section is provided in detail for a one-channel eikonal formulation, alongside with comparison with all available data.

Our model is not in conflict with the dominant analytic description of total, and elastic cross section based on Regge-Pomeron models such as for instance [6] or [7], rather it provides an intuitive description of hadronic scattering in terms of low  $p_t$  collisions describable by perturbative QCD and soft gluon emission, for which a mixed approach, perturbative and non-perturbative is required.

## II. SOFT EDGE AND MINI JETS

These are two basic *facts* about the  $pp$  and  $p\bar{p}$  total cross section:

- $\sigma_{total}$  first decreases and then, around  $\sqrt{s} \simeq (10 \div 20)$   $GeV$  rises as a function of the squared cm energy  $s$ .
- $\sigma_{total}$  asymptotically cannot rise faster than  $\log^2[s/s_0]$

Both phenomena have a physical interpretation in terms of QCD, the difficulty lies in a proper implementation of the second fact. We shall start, in this section, from the first *fact*, in particular the rise, which appears when gluon-gluon scattering becomes observable. This argument can be made quantitative.

At low CM energy, soft gluon emission accompanying non-perturbative effects decreases the cross section, while there are not enough perturbative gluons for beam-on-beam scattering. However, as the energy increases, more energy is available for gluon emission, and there is a non-zero probability for hard gluon-gluon scattering with production of final state partons of  $p_t \sim 1$   $GeV$ . For such energy regions, the collision can be described by perturbative QCD through the asymptotic freedom expression for the coupling,  $\alpha_{AF}(p_t^2)$ , valid when  $p_t^2 \gg \Lambda_{QCD}^2$ . The emission of hard gluons is a perturbative process, characterized by a  $1/x \sim \sqrt{s}/(2p_t)$  parton spectrum. As the energy increases

further, the cross section for collisions resulting with a final state parton with  $p_t \gtrsim 1$ , will start rising because of  $1/x$  behavior, entering into a *high gluon luminosity* region. We see that the contribution to the total cross section from these hard collisions can become sizable and rising with energy when

$$1/x = \sqrt{s}/2p_t \gg 1 \text{ and } p_t > 1 \text{ GeV.} \quad (1)$$

With the condition  $p_t > 1 \text{ GeV}$  for the *asymptotic freedom condition* to be satisfied, and the rise starting when  $x \ll 1$ , for instance  $\simeq 0.1 - 0.2$ , the turning point for the rise to start is for

$$\sqrt{s} \gtrsim (2/x) \text{ GeV} \quad (2)$$

$$\sqrt{s} \sim (10 \div 20) \text{ GeV} \quad (3)$$

as the data show. The transition from collisions which do not involve scattering of perturbative gluons, to a region dominated by mini-jets, is what is seen in the total cross section data, and is discussed, in a somewhat different language, in [1].

The above argument can be made quantitative by calculating the bulk of perturbative gluon-gluon collisions, i.e. the mini jet cross section. The mini-jet cross section is given by

$$\sigma_{\text{jet}}^{AB}(s; p_{t\min}) = \int_{p_{t\min}}^{\sqrt{s}/2} dp_t \int_{4p_t^2/s}^1 dx_1 \int_{4p_t^2/(x_1 s)}^1 dx_2 \sum_{i,j,k,l} f_{i|A}(x_1, p_t^2) f_{j|B}(x_2, p_t^2) \frac{d\hat{\sigma}_{ij}^{kl}(\hat{s})}{dp_t}. \quad (4)$$

where  $f_{i|A}(x_1, p_t^2)$  are the PDFs with  $i, j, k, l$  to denote the partons and  $x_1, x_2$  the fractions of the parent particle momentum carried by the parton.  $\sqrt{\hat{s}} = \sqrt{x_1 x_2 s}$ ,  $\hat{\sigma}$  are the center of mass energy of the two parton system and the hard parton scattering cross-section respectively. Following the argument given above, this expression sums only collisions with outgoing partons of momentum with  $p_t > p_{t\min}$ , where  $p_{t\min}$  is defined as the region of validity of perturbative QCD, i.e. the coupling is given by the asymptotic freedom expression for running  $\alpha_F$ . Different

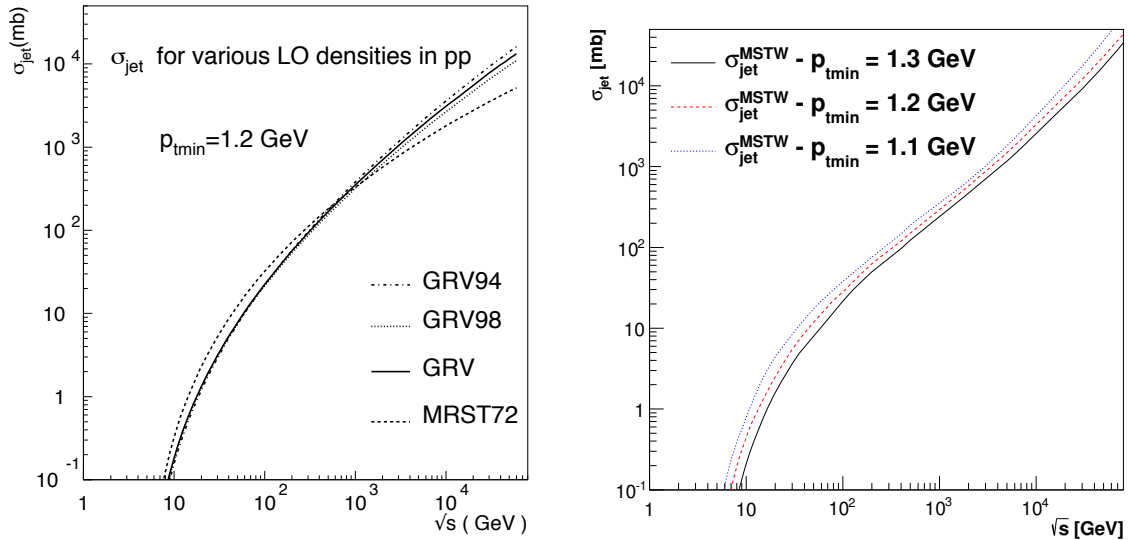


FIG. 1. Integrated mini jet cross section for GRV (older) densities [8–10] or MRST72 [11], and a fixed chosen  $p_{t\min}$  value (left), and with MSTW2008 [12] LO PDFs (right) for a range of  $p_{t\min}$  values showing a distinct change of behavior, from a very fast rise to a power law, around  $\sqrt{s} \simeq (10 \div 20) \text{ GeV}$ .

densities give rise to different energy dependence of the mini jet cross section, as they differ in

their very low- $x$  behavior. In Fig. 1 we display the energy -dependence of  $\sigma_{jet}(s)$ , with parameter choices corresponding to  $p_{tmin} \simeq 1 \text{ GeV}$  and different PDFs. We use LO current PDFs DGLAP evolved, from PDF libraries. A clear threshold behavior appears around ISR energies and confirms the mini-jet explanation of the *soft edge*, that is, for  $\sqrt{s} \gtrsim 10 - 20 \text{ GeV}$  the cross section rises mainly due to the energy evolution of the proton "radius", coming from emergent gluon-gluon hard scatterings.

For a fixed  $p_{tmin}$ , these mini-jet cross sections rise as a power law,  $s^{0.3-0.4}$ , and, when included in the formalism for the total cross section, phenomenologically correspond to the hard Pomeron of Regge-Pomeron models.

For the transition to be at the  $\sqrt{s}$  values as indicated by the rise of the cross section at ISR, the parameter  $p_{tmin}$  has to be roughly energy independent. This is in disagreement with other, typically Regge-Pomeron, formulations, but is in agreement with the observation in [1] and confirms the finding of our model, which, from the very beginning, used a constant  $p_t$  value, labelled as  $p_{tmin}$ , as a divider between scattering giving rise to mini-jets and non-perturbative scattering.

However, this poses a serious problem with the rigorous limits imposed on cross sections by the Froissart bound. In various mini-jet or Regge-Pomeron based models, this is the main reason to introduce an energy dependent  $p_{tmin}$ . In so doing however, not only there is no way to simply explain the *soft edge* as a fixed energy threshold, but an important piece of physics remains hidden, namely soft gluon re-summation that tames the unphysical rise of the mini-jet cross section. To which we now turn.

### III. SOFT GLUON RE-SUMMATION AND THE FROISSART BOUND

We now turn to the *second fact* mentioned earlier. In our model the softening of the rise is obtained by soft gluon emission, a phenomenon always accompanying hard scattering, such as the one which results in the mini-jet production. Our starting point is that resummed soft gluon emission tames the rise of the mini-jet cross section. Soft emission always decreases the observable cross section, since it introduces an overall transverse momentum  $K_t \neq 0$  in the center of mass of the colliding particles, namely it leads to acollinearity of the initial particles in the scattering. We have suggested that soft gluon QCD re-summation plays the same effect in hadron-hadron collisions, in particular accompanying hard parton-parton scattering. In [13], we advanced the conjecture that such phenomenon is behind the initial decrease of total cross sections, before the on-set of mini jets. Past ISR, perturbative QCD effects, i.e. mini jets, take over, and the combination of the decrease due to soft gluon re-summation (SGR) and the rise of mini-jets transforms the rapid power law rise into a milder behaviour, leading to the second important *fact* mentioned in Sect.II.

A quantitative description of this mechanism poses an extraordinary challenge, and we shall here briefly outline how we have approached the problem in our model [14].

We consider the following standard expression for soft  $k_t$  re-summation, i.e.

$$\frac{d^2 P(\mathbf{K}_t)}{d^2 \mathbf{K}_t} = \frac{1}{(2\pi)^2} \int d^2 \mathbf{b} e^{i\mathbf{K}_t \cdot \mathbf{b}} e^{-h(\mathbf{b})} \quad (5)$$

$$h(\mathbf{b}) = \int d^3 \bar{n}(k) [1 - e^{-i\mathbf{k}_t \cdot \mathbf{b}}] \quad (6)$$

where  $d^3 \bar{n}(k)$  is the average number of soft quanta emitted during a collision. In our model, the Fourier transform of the above expression describes the impact parameter distribution of partons in the proton,  $A(b, s)$ , during the hard gluon-gluon collision. In the well known formulation of SGR [15, 16], the lower limit of the  $k_t$  integration is excluded, via an infrared cutoff of order  $\Lambda_{QCD}$ . This procedure is acceptable as long as there is no singularity in the infra-red region [16], which is certainly not true when confinement effects play a role.

Our model relies on an adequate, albeit phenomenological, inclusion of *the infra-red region*. We parametrize the very low  $k_t$  emission with a parameter  $p$ , through an effect of zero momentum

or close to zero momentum emission. Our parametrization of the infra-red(IR) region has been discussed at length in many publications, see for instance [5] and [13], and will not be repeated here, except to remind the reader that it basically amounts to describe the IR region through a singular but integrable expression for the coupling  $\alpha_{eff}$  of very soft, infra-red gluons from the emitting quark current, namely we use

$$\alpha_{eff} = \frac{12\pi}{33 - 2N_f} \frac{p}{\log[1 + p(k_t/\Lambda_{QCD})^{2p}]} \quad (7)$$

The parameter  $p$  regulates the singularity, it is by construction  $1/2 < p < 1$ . We determine its value phenomenologically, but we expect it to be related to the coefficient of the beta function. With such an expression,  $k_t$ -resummation in transverse momentum of soft gluons emission can be performed down into the  $k_t = 0$  region.

We label the impact parameter distribution accompanying mini-jet scattering with the subscript BN as  $A_{BN}^{pp}(p, PDF; b, s)$ , pinpointing to the need for re-summation of soft quanta emitted in the so-called infrared catastrophe [17]. We have

$$A_{BN}^{pp}(p, PDF; b, s) = \frac{e^{-h(p; b, s)}}{\int d^2\mathbf{b} e^{-h(p; b, s)}} \quad (8)$$

$$h(b, s; p) = \frac{16}{3\pi} \int_0^{q_{max}} \frac{dk_t}{k_t} \alpha_{eff}(k_t) \log \frac{2q_{max}}{k_t} [1 - J_0(bk_t)] \quad (9)$$

$$\alpha_{eff}(k_t) \propto \left(\frac{k_t}{\Lambda}\right)^{-2p} \quad k_t \rightarrow 0 \quad (10)$$

where the upper limit of integration  $q_{max}$  indicates the PDF dependence, as we see shortly. We have discussed the above distribution in many publications, starting with [14]. Its main characteristic is to include soft gluon re-summation down to  $k_t = 0$ , and regulate the infrared singularity through a parameter  $p$ , so as correspond to a dressed gluon potential  $V \sim r^{2p-1}$  for  $r \rightarrow \infty$ . We have also shown an important consequence of an expression such as the above for  $\alpha_{eff}(k_t \rightarrow 0)$  [18], namely that, asymptotically, the regularized and integrated soft gluon spectrum of Eq. (9) is seen to rise as

$$h(b, s; p) \rightarrow (b\bar{\Lambda})^{2p} \quad (11)$$

and the  $b$ -distribution  $A_{BN}^{pp}$  exhibits a cut-off in  $b$ -space strongly dependent on the parameter  $p$ . When the above distribution is included in an eikonal mini jet model, such cut-off is seen to give rise to a total cross section which rises asymptotically as  $[\log s]^{1/p}$ , as shown in [18], where details can be found.

Phenomenologically, just as the mini-jet cross section depends on the PDFs, so will the soft gluon spectrum accompanying the hard scattering and so will the expression we propose for the impact parameter distribution of partons. This happens through the maximum transverse momentum allowed to single soft gluon emission during the hard gluon-gluon collision. The dynamical scale  $q_{max}(s)$  in Eq. (9) is obtained from the kinematics for single soft gluon emission [19]. In our model, as discussed in the original formulation [5], we have made some approximations, such as that most contributions come from  $p_t \simeq p_{tmin}$ , and have then taken averages over the densities chosen for the mini-jet cross section. Thus, we use the expression

$$q_{max}(s; p_{tmin}) = \frac{\sqrt{s}}{2} \frac{\sum_{i,j} \int \frac{dx_1}{x_1} \int \frac{dx_2}{x_2} \int_{z_{min}}^1 dz f_i(x_1) f_j(x_2) \sqrt{x_1 x_2} (1-z)}{\sum_{i,j} \int \frac{dx_1}{x_1} \int \frac{dx_2}{x_2} \int_{z_{min}}^1 dz f_i(x_1) f_j(x_2)} \quad (12)$$

with  $z_{min} = 4p_{tmin}^2/(sx_1x_2)$ .<sup>1</sup> This scale, the maximum transverse momentum allowed for single soft gluon emission at a given energy, has a strong dependence on the PDFs used for its calculation,

<sup>1</sup> A typo in Eq. 12 has been corrected wrt to the ArXiv v2 and published PRD version.

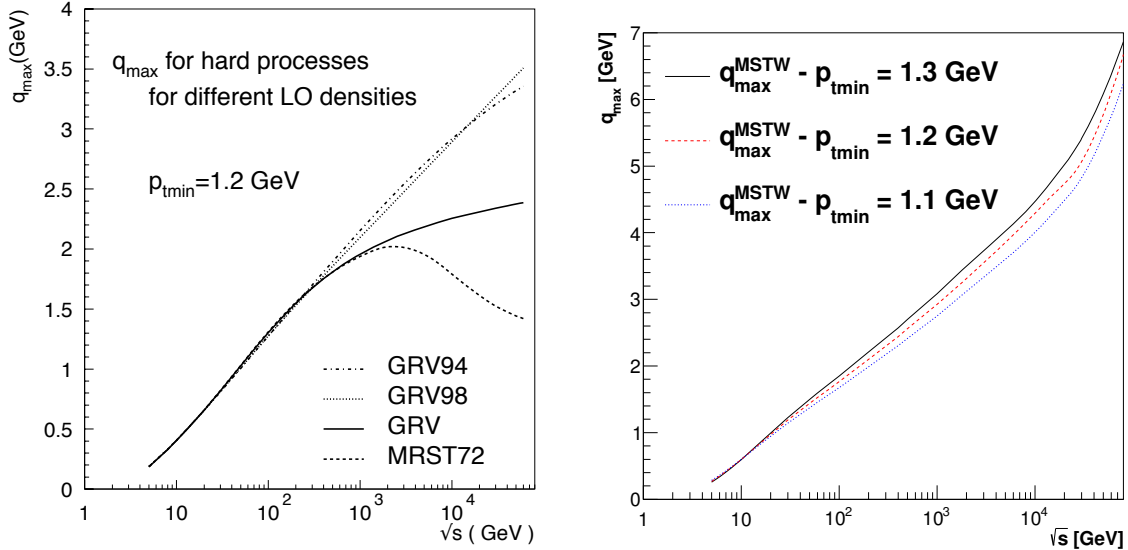


FIG. 2. Dynamically generated scale  $q_{\max}$  for different PDFs and a fixed  $p_{t\min}$  value (left panel) and MSTW2008 LO parton densities, within a range of  $p_{t\min}$  values.

and on  $p_{t\min}$ , as well. In this paper we shall show results for different LO PDFs. In previous publications [3], we discussed the case of GRV [8–10], or MRST72 [11]. In the left panel of Fig. 2 we show the  $s$ -dependence of the soft energy scale  $q_{\max}$  for these densities and for one fixed value of  $p_{t\min}$ . New updated densities are now available, and we show in the right hand panel the  $s$ -dependence for a range of values for  $p_{t\min}$  and for the recent LO PDF set, MSTW2008, for brevity also called MSTW in this paper [12]. Thus, while the scale defining the mini jet contribution, i.e.  $p_{t\min}$ , is fixed, the model has a dynamically generated energy dependent scale,  $q_{\max}$ .

#### IV. ONE-CHANNEL MINI-JET MODEL FOR TOTAL, ELASTIC AND INELASTIC CROSS SECTIONS

The appearance of mini-jets in hadronic collisions has a long history [20]. The construction of the total hadronic cross section with mini-jets had started in [21] with a simple model with an energy dependent  $p_{T\min}(s)$ . The original suggestion in [21] did not use the eikonal representation, and was based on phenomenologically determined values of  $p_{T\min}(s)$  at different energies. Embedding the mini-jets in the eikonal formulation [22], unitarity would be automatically satisfied but the modeling increased due to the request of specifying an impact parameter distribution. Durand and Pi's original suggestion and many others to follow, use the one-channel description, but their use is limited and in what follows we shall clarify these limitations.

Presently, good descriptions of all the components of the cross section are obtained through multi-channel formulations. Some of them [23] are discrete *à la Good and Walker* [24], others are based on a continuous [25, 26]. The price to pay then is addition of more free parameters. Current models in perturbative QCD, on accounting for multiple Pomeron interactions, invoke enhanced “fan” diagrams [27–29] which require the knowledge of non-linear coupling between Pomerons. Non-linear equations such as the Balitsky-Kovchegov (BK) equation [30, 31], are used to describe these non-linear contributions to diffraction. Such non-linear couplings become important when the gluon momentum becomes very small, a region insofar unreachable by perturbative QCD. Thus, while diffraction needs a multichannel approach, its complete description and phenomenology so

far have to rely on more parameters [32], some of which embody the non-linear behavior in the unknown infrared region.

In this section, we shall discuss the mini-jet contribution to total, elastic and inelastic cross section, using a one-channel eikonal formulation, and leave to a forthcoming publication, the implementation to a general model and the inclusion of diffractive processes.

#### IV.1. The total cross section

In this section, we shall update our mini jet model results to LHC13 energies and beyond. To construct the total cross section, mini-jets are embedded into the eikonal formulation. Starting with

$$\sigma_{total} = 2 \int d^2\vec{b} [1 - \Re(e^{i\chi(b,s)})] \quad (13)$$

and neglecting the real part in the eikonal at very high energy, the above expression further simplifies into

$$\sigma_{total} = 2 \int d^2\vec{b} [1 - e^{-\chi_I(b,s)}] \quad (14)$$

where  $\chi_I(b,s) = \Im m \chi(b,s)$ . Notice that  $\Re \chi(b,s) \simeq 0$  is a reasonable approximation for the scattering amplitude in  $\mathbf{b}$ -space at  $t = 0$ , where very large values of the impact parameter dominate and phenomenologically the ratio of the real to the imaginary part of the forward scattering amplitude  $\rho(s) \ll 1$ . By properly choosing a function  $\chi_I(b,s)$ , all total hadronic cross sections,  $pp$ ,  $p\bar{p}$ ,  $\pi p$ , etc., can be described up to currently available data [33]. In the vast majority of models, new data have often required an adjustment of the parameters which give  $\chi_I(b,s)$ .

In previous publications, we had proposed a band whose upper border gave a good prediction for LHC results. By updating the model and anchoring the parameter set to LHC results, one can now proceed to refine our predictions for higher energies, LHC13 and beyond to the cosmic rays region. The eikonal function of the mini-jet model of [5, 13] is given by

$$2\chi_I(b,s) = n_{soft}^{pp}(b,s) + n_{jet}^{pp}(b,s) = A_{FF}(b)\sigma_{soft}^{pp}(s) + A_{BN}^{pp}(p,PDF;b,s)\sigma_{jet}(PDF,p_{tmin};s) \quad (15)$$

The first term includes collision with  $p_t \leq p_{tmin} \sim (1 \div 1.5) \text{ GeV}$ , the second is obtained from the mini-jet cross section. The term  $n_{soft}^{pp}(b,s)$  is not predicted by our model so far and we parametrize it here with  $\sigma_{soft}^{pp}(s)$ , obtained with a constant and one or more decreasing terms, and  $A_{FF}$ , the impact parameter distribution in the non perturbative term, obtained through a convolution of two proton form factors.

As we have seen, the second term in Eq.(15) is numerically negligible at energies  $\sqrt{s} \lesssim 10 \text{ GeV}$ . The perturbative, mini-jet, part discussed previously is defined with  $p_t^{parton} \geq p_{tmin}$  and is determined through a set of perturbative parameters for the jet cross section, namely a choice of PDFs and the appropriate  $p_{tmin}$ . Since soft gluon re-summation includes all order terms in soft gluon emission, our model uses LO, library distributed, PDFs.

In our previous publications [2, 3], we have reproduced data for  $pp$  and  $p\bar{p}$ , up to the Tevatron results. However, the large differences among the Tevatron measurements did not allow a precise description at higher energies, such as those at LHC. Therefore we have updated our analysis, using only  $pp$  data, ISR and the recent LHC measurements, and including a more recent set of LO densities, MSTW2008 [12]. The values of  $p$  and  $p_{tmin}$  which better reproduce the LHC result are obtained by varying  $p_{tmin} \simeq 1 \div 1.5 \text{ GeV}$  and  $1/2 \lesssim p \lesssim 0.8$ . The result, for the total  $pp$  cross sections, is shown in Fig. 3. The  $p\bar{p}$  points are shown, but have not been used for the phenomenological fit. Cosmic ray extracted values for  $pp$  have not been used either. We have included the curves corresponding to GRV densities and compared our model with other

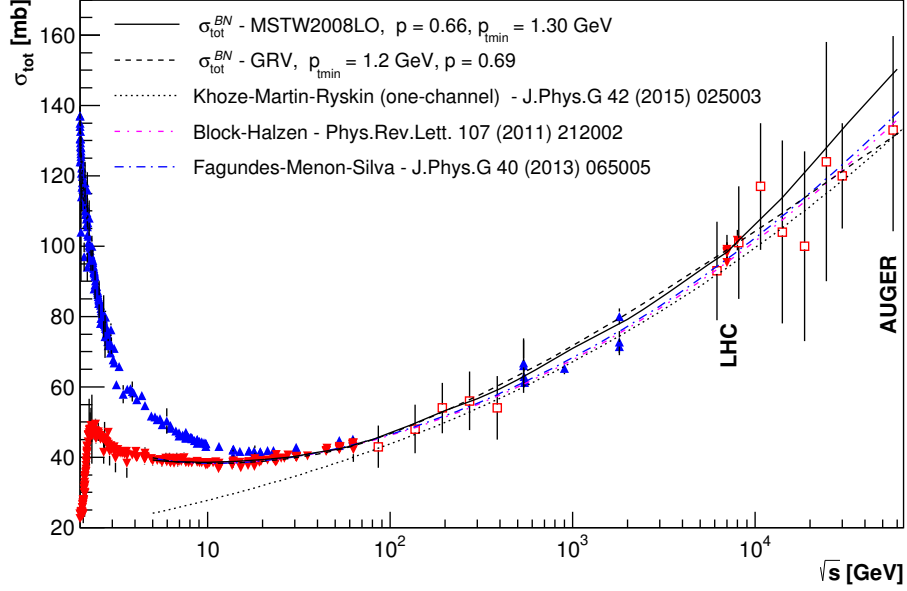


FIG. 3. QCD mini-jet with soft gluon resummation model and  $pp$  total cross section. Accelerator data at LHC include TOTEM [34, 35] and ATLAS measurements [36]. Neither  $\bar{p}p$  nor the cosmic ray data points have been used for the calculation. Our results are shown with predictions in the high cosmic ray region obtained with two types of densities, GRV and MSTW, and they are compared with one-channel model from Khoze et al.[7]. The red *dot-dashed* curve corresponds to fits to the total cross section by Block and Halzen [37], the dot-dashed blue line represents the fit by Fagundes-Menon-Silva [38].

predictions [7, 37, 38]. Table I contains the points corresponding to our model results for both GRV and MSTW2008 densities.<sup>2</sup> Results for MRST72 densities can be found in [39], together with details of different parameter sets used for the different PDFs.

TABLE I. Total cross section values in mb, from the mini-jet model with two different PDFs sets.

$\sqrt{s}$ GeV	$\sigma_{total}^{GRV}$ mb	$\sigma_{total}^{MSTW}$ mb
5	39.9	39.2
10	38.2	38.6
50	41.9	42.2
500	63.2	62.0
1800	79.5	77.5
2760	85.4	83.6
7000	98.9	98.3
8000	100.9	101.3
13000	108.3	111.7
14000	109.3	113.7
57000	131.1	149.2

We notice that our model is able to describe very well all the total cross section accelerator data, and gives a good agreement with cosmic ray data. The AUGER point falls within the two different

<sup>2</sup> In the arXiv v2 and in the published PRD paper, there were errors in the table for MSTW predictions at 13 and 57 TeV. These have now been corrected.



parameterizations we are using, full line for MSTW and dashes for GRV. By construction, both parameterizations remain very close up to LHC7 and LHC8 energies, and start diverging as the energy increases, as a consequence of the uncertainty on the very low- $x$  behavior of the densities.

To summarize the results of this section, in the model we have proposed, past ISR energies mini-jets appear as hard gluon-gluon collisions accompanied by soft gluon emission  $k_t$ -resummed down into the infrared region. In this language, we have a *dressed* hard scattering process, with the mini-jet cross section giving the same energy behavior as the hard Pomeron, and soft gluon resummation providing *the dressing*, in which the hard interaction is embedded. The eikonal formulation then transforms this *dressed hard gluon* interaction into a unitary ladder. The main difference with other mini-jet models such for instance in [40], is the taming mechanism ascribed to soft gluon resummation in the infrared region.

#### IV.2. One-channel eikonal mini jet models and the inelastic cross section

The inelastic total cross section is defined by subtraction from the total and the elastic cross sections. However, experimentally, it is usually defined only in specific phase space regions, and eventually extrapolated via MC simulation programs, which also include parameters and choice of models in the diffractive region. One exception is TOTEM which covers a large rapidity range. In this subsection, we shall focus on one, theoretically well defined, part of the inelastic cross section, what we define as *uncorrelated*, which is appropriately described in the mini-jet context and through the one-channel mode. In the following we shall see how.

Since our study [3] on the inelastic cross section at LHC, soon followed by the first experimental results [41], data related to measurements in different kinematic regions have appeared. Extensive and detailed measurements have been obtained for the inelastic proton-proton cross section by CMS [42], ATLAS [41], TOTEM [35, 43], ALICE [44] and LHCb [45] Collaborations. These measurements cover different regions, central and mid-rapidity, large rapidity, high and low mass diffractive states. Extensive QCD modeling, including minijets [46–49], goes in describing the different regions.

Here, we consider the implication of any given one-channel eikonal model. Thus, we repeat the argument about the relation between the Poisson distribution of independent collisions and diffractive processes given in [3], where we stressed that the inelastic cross section in a one-channel eikonal model coincides with the sum of independently (Poisson) distributed collisions in  $b$ -space. Namely, with

$$\sigma_{total} = \sigma_{elastic} + \sigma_{inel} \quad (16)$$

then, in a one-channel (*one-ch*) mode,

$$\sigma_{inel}^{one-ch} \equiv \sigma_{tot} - \sigma_{elastic}^{one-ch} = \int d^2\mathbf{b} [1 - e^{-2\chi_I(b,s)}] \quad (17)$$

But since

$$\sum_1^{\infty} \frac{(\bar{n})^n e^{-\bar{n}(b,s)}}{n!} = 1 - e^{-\bar{n}(b,s)} \quad (18)$$

one can identify the integrand at the right hand side of Eq. (17) with a sum of totally independent collisions, with  $2\chi_I(b,s) = \bar{n}(b,s)$ . We suggest that this means that in so doing one excludes diffraction and other quasi-elastic processes from the integration in Eq. (17). Hence, the simple splitting of the total cross section as in Eq. (16) needs to be better qualified when a one-channel eikonal is used. In such a case, the “elastic” cross section

$$\sigma_{elastic}^{one-ch} = \int d^2\vec{b} |1 - e^{-\chi_I(b,s)}|^2 \quad (19)$$

must be including part of the inelastic contribution, i.e.

$$\sigma_{elastic}^{one-ch} = \sigma_{elastic} + \text{diffractive or otherwise correlated processes} \quad (20)$$

and  $\sigma_{inel}^{one-ch}$  is only the non-diffractive part. Within this approach, we can compare Eq. (17) with data.

This comparison is shown in Fig. 4, where the present inelastic cross section data up to AUGER energies [50] are plotted. The blue band corresponds to the expectations from Eq. (17) where the same eikonal function  $\chi_I(b, s)$  which gives the total cross section of Fig. 3 is used. Having anchored the eikonal  $\chi_I(b, s)$  to the LHC total cross section, the band indicates the spread of predictions due to the different asymptotic low- $x$  behavior of the employed densities, as the energy increases beyond LHC8. The top curve corresponds to MSTW2008, the lower one to GRV.

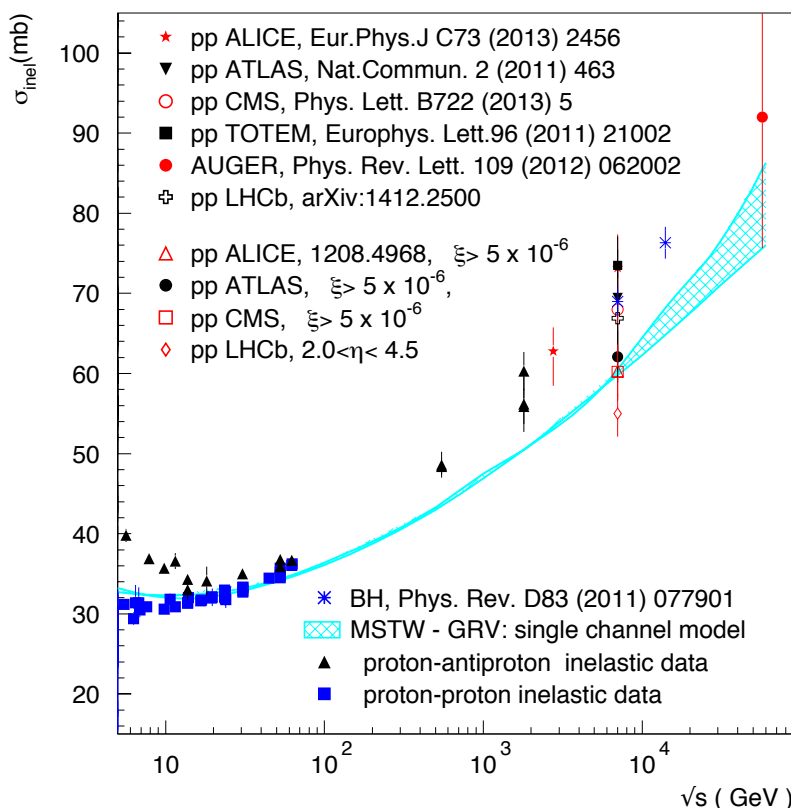


FIG. 4. Data for the inelastic cross section and comparison with GRV and MSTW2008 densities in the present one-channel mini-jet model. We also show comparison with Bloch and Halzen (BH) results [51].

The comparison with experimental data is very interesting. While the present LHC inelastic cross section data span a range of values corresponding to different kinematic regions, Eq. (17) identifies the region where uncorrelated events described by mini-jet collisions, parton-parton collision with  $p_t > p_{tmin}$ , play the main role. From the comparison with data, we can identify it with the region  $\xi = M_X^2/s \geq 5 \times 10^{-6}$  where three LHC experiments, ATLAS [41], CMS [42] and ALICE [44], agree to a common value within a small error. This measurement is in the high mass region (for

instance, at LHC7 the lower bound gives  $M_X = 15.7 \text{ GeV}$ ). LhCb results correspond to a lower cross section, but they do not cover the same region of phase space.

The results of this and of the previous subsection are summarized in Fig. 5 where the bands correspond to different PDFs used in the calculation of mini-jets and to their different extrapolation to very low- $x$  at the cosmic ray energies.

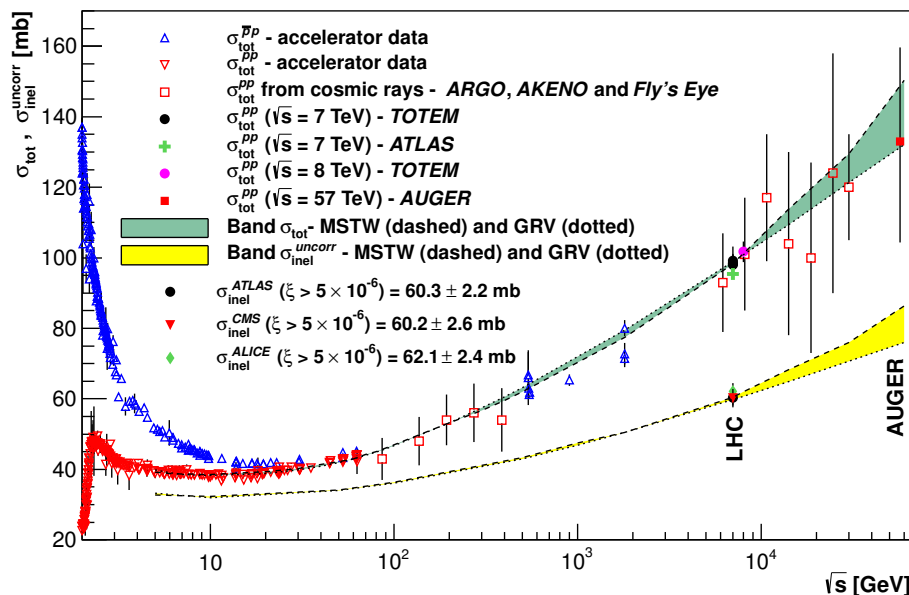


FIG. 5. Results for our eikonalized QCD mini-jet with soft gluon resummation model are shown for  $pp$  total cross section and for the inelastic uncorrelated part of the inelastic cross section. Accelerator data at LHC include TOTEM [34, 35] and ATLAS measurements [36]. The inelastic uncorrelated cross section is compared with inelastic processes for  $M_X^2/s > 5 \times 10^{-6}$  as measured by ATLAS [41], CMS [42] and ALICE [44]. The green and yellow bands give the uncertainty following use of different PDFs sets, MSTW2008 and GRV, as also shown in [39].

The dashed yellow band is the one-channel inelastic cross section that only includes Poisson-distributed independent scatterings. That is, once the parameters of the eikonal  $\chi_I(b, s)$  are chosen to give an optimal reproduction of the the total cross section, the computed inelastic cross section immediately gives the uncorrelated part of the total inelastic cross section. The importance of this fact for cosmic ray deduced  $pp$  cross sections has been noticed in [39] and shall be examined further elsewhere.

### IV.3. Diffractive, elastic and inelastic cross sections reexamined

The total cross section, which our model successfully describes, includes different components, but only one of them is well defined experimentally as well as theoretically, that is the elastic cross section. It is well known that one-channel eikonal models fail to simultaneously describe the total and the elastic cross section through the entire available CM energy range, with the same parameter set. In the last sub-section, we have delineated this shortcoming through the observation that once minijets become operative past the *soft edge*, the computed elastic cross section includes correlated inelastic collisions and the computed inelastic lacks the same (i.e., its correlated inelastic part). We now discuss this matter in detail so as to make these statements quantitative. We shall do so through the one- channel mini-jet model with a suitable parametrization of diffractive data.

In one- channel eikonal models, with the inelastic part given by Eq. (17), the elastic part of the total cross section is given by Eq. (19). Notice that whereas Eq. (17) is exact, in Eq. (19) the real part of the eikonal function has been neglected, as in Eq. (13).

Eq. (19) reproduces with a good approximation the elastic cross section data up to the onset of minijets, deviating significantly from the data already at energies  $\sim 100$  GeV. In particular, at the Tevatron, Eq. (19) gives an elastic cross section roughly 30 % higher than the data. This is shown in the left hand plot of Fig. 6, where the one-channel result from Eq. (19) is plotted together with elastic scattering data and an empirical parametrization of all elastic differential cross section  $pp$  data from ISR to LHC7 [52]. This parametrization leads to the expression

$$\sigma_{elastic} = At_0 e^{Bt_0} E_8(Bt_0) + \frac{C}{D} + 2\sqrt{AC} \cos \phi t_0 e^{(B+D)t_0/2} E_4\left(\frac{(B+D)t_0}{2}\right), \quad (21)$$

where

$$E_n(x) = \int_1^\infty \frac{e^{-xy}}{y^n} dy. \quad (22)$$

The model of [52] is based on the well known Phillips and Barger model [53] for the elastic differential cross section, implemented by a form factor term to fully reproduce the optical point, and hence the total cross section, as well as the forward slope. Through suitable predictions for the high energy behavior of the parameters, the parameterization of [52] provides a model independent prediction both for elastic and total cross sections at very high energies, and hence can be used as a good test of different models in the high energy region beyond present accelerator data.

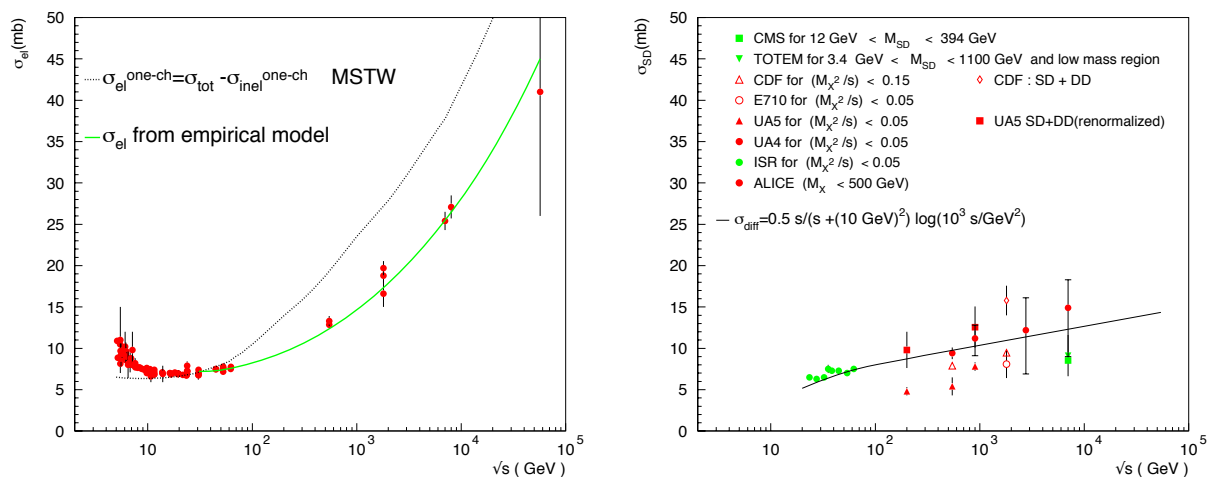


FIG. 6. At left, we show the elastic  $pp$  cross section from the one-channel mode given by the dotted curve, with choice of MSTW2008 PDF as in the upper curve of Fig. 3. The green curve corresponds to an empirical parametrization of all differential elastic  $pp$  data [52]. Comparison is done with both  $pp$  and  $p\bar{p}$  data. The right hand panel shows diffraction data from E710 [54], UA5 [55, 56], UA4 [57], ISR [58], CDF [59], CMS [60], TOTEM [35] and ALICE [44] compared with the parametrization given by Eq. (23) mentioned in the text.

The left hand plot of Fig. 6 shows that at low energies, before the onset of mini-jets, one- channel models may be used to describe both elastic and total cross sections. However, past ISR energies the threshold of perturbative QCD, reflected in the appearance of the *soft edge*, is crossed, and one-channel models fail. One-channel models are also unable to reproduce the behaviour of the

differential elastic cross section, and multichannel models with added parameters are then needed to describe diffraction. The difficulty with proper descriptions of diffraction is that at different energies, different parts of the phase space are accessed by different experimental set-ups, as we show in the right hand plot of Fig. 6. For the argument to follow, we consider an estimate of  $\sigma_{Diff}$  given by Eq. (36) of [61], which provides a good interpolation of Single Diffractive (SD) data, from ISR to the LHC results from ALICE, CMS and TOTEM, as we shown in Fig. 6. i.e.

$$\sigma_{Diff}(s) = \left[ \frac{(0.5mb) s}{s + (10 \text{ GeV})^2} \right] \log\left(\frac{10^3 s}{\text{GeV}^2}\right), \quad (23)$$

We have adopted this parameterization for the full diffractive component at high energy. This is an approximation, justified at very high energy by the TOTEM result for Double Diffraction(DD) [62], namely  $\sigma_{DD} \simeq 0.1mb$ , although this result was obtained in a narrow range of pseudo rapidity and more data are needed to conclude that DD does not play a significant role at LHC energies. At lower energy the definitions vary, as we show in this figure.

We shall now show how the one-channel mini-jet model presented here can be used to predict the full inelastic cross section at higher energies.

We start with the elastic cross section, and consider now the difference

$$\sigma_{elastic}^{one-ch} = \sigma_{tot} - \sigma_{inel}^{one-ch} \quad (24)$$

which includes diffractive (otherwise said, correlated inelastic) contribution, as also discussed in general terms in [63], among others. If

$$\sigma_{inel} = \sigma_{inel}^{one-ch} + \sigma_{Diff} \quad (25)$$

then, we should be able to obtain the measured elastic cross section from

$$\sigma_{elastic} = \sigma_{elastic}^{one-ch} - \sigma_{Diff} \quad (26)$$

We compare the procedure outlined through Eqs. (23) and (26) with experimental data and with the empirical parametrization of Eq. (21). The result is shown in the left panel of Fig. 7. We see that such a procedure gives a good description of the elastic cross section at high energy, basically past the CERN  $SppS$ .

Likewise, from Eq. (25), we can see that by adding the diffractive part, parametrized as in Eq. (23), to the prediction from the one-channel model, it is possible to obtain a good description of the high energy behavior of the inelastic cross section. This is shown in the right hand panel of Fig. 7. It must be noticed that this procedure shows agreement with data only past ISR energies (in fact from  $SppS$  onwards) energies and that a model describing both the low and the high energy will have to go beyond the one-channel exercise described here. In Table II, we show the predictions from this model for the inelastic cross section at LHC13,  $\sqrt{s} = 13 \text{ TeV}$ .<sup>3</sup>

TABLE II. Minijet model predictions for the inelastic cross section at  $\sqrt{s} = 13 \text{ TeV}$ . Predictions of  $\sigma_{inel}$  in the full phase-space were obtained by adding  $\sigma_{diff}(13 \text{ TeV}) = 12.9 \text{ mb}$  to  $\sigma_{inel}^{uncorr} \equiv \sigma_{inel}^{one-ch}$ .

<i>PDF</i>	$\sigma_{inel}^{uncorr}$ (mb)	$\sigma_{inel}$ (mb)
<i>GRV</i>	64.3	77.2
<i>MSTW</i>	66.9	79.8

The result of this subsection confirms the interpretation that at high energies, past the beginning of the rise and the onset of mini-jets, the one-channel inelastic cross section is devoid of most of the diffractive contribution.

<sup>3</sup> In the arXiv v2 and in the published PRD version, this table had an error in the MSTW predictions at  $\sqrt{s} = 13 \text{ TeV}$ . It has now been corrected.

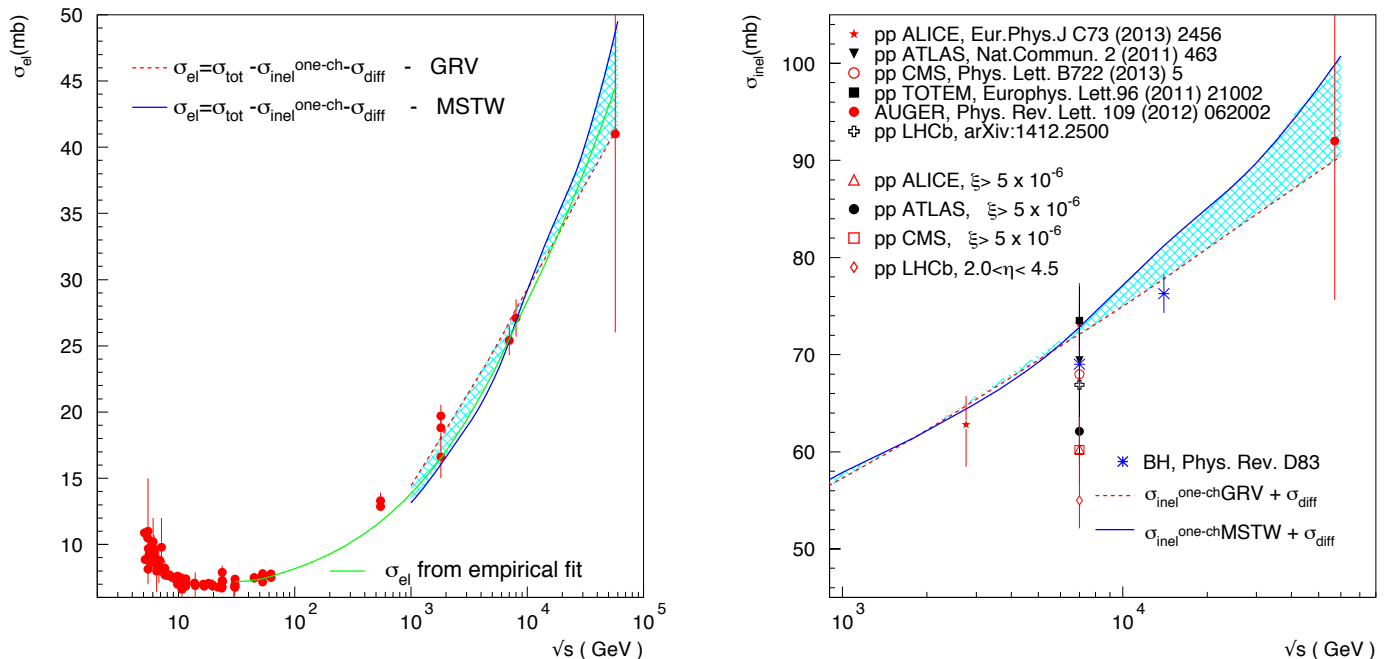


FIG. 7. Left panel: the total elastic cross section obtained by subtracting Single Diffractive contributions, indicated as  $\sigma_{diff}$ , from the one- channel model result. The resulting curve is compared with  $pp$  and  $p\bar{p}$  data and the empirical parametrization of [52], which is seen to fall within the two model predictions. The right panel shows the corresponding exercise for the inelastic cross section: at high energies, adding diffraction brings the one-channel result in agreement to data.

## V. SUMMARY AND CONCLUSIONS

We have shown that the onset and rise of the mini-jet cross section provide the dynamical mechanism behind the appearance of a *soft-edge* [1], i.e., a threshold in the total cross section around  $\sqrt{s} \simeq (10 \div 20) \text{ GeV}$ . Thus, our model for the total  $pp$  cross section that utilizes mini-jets with soft-gluon re-summation has a built in soft-edge. It has been updated with recent PDFs for LHC at  $\sqrt{s} = 7, 8 \text{ TeV}$  and predictions made for higher energy LHC data and cosmic rays.

We have also discussed in detail the reasons behind failures to obtain correct values for the elastic cross sections from a one-channel eikonal that obtains the total cross section correctly. It has been shown, through the use of phenomenological descriptions of diffractive (otherwise said, correlated inelastic) cross sections, that one-channel elastic cross section is indeed a sum of the true elastic plus correlated inelastic cross sections. An application of this fact to cosmic ray data analysis for the extraction of  $pp$  uncorrelated-inelastic cross sections shall be presented elsewhere.

## ACKNOWLEDGMENTS

We thank Simone Pacetti for collaboration about the empirical model results. A.G. acknowledges partial support by Junta de Andalucia (FQM 6552, FQM 101). D.A.F. acknowledges the São Paulo Research Foundation (FAPESP) and CAPES for financial support (contract: 2014/00337-8). O.S. acknowledges partial support from funds of Foundation of Polish Science grant POMOST/2013-

7/12, that is co-financed from European Union, Regional Development Fund.

- 
- [1] M. M. Block, L. Durand, F. Halzen, L. Stodolsky, and T. J. Weiler, Phys.Rev. **D91**, 011501 (2015), arXiv:1409.3196 [hep-ph].
  - [2] A. Achilli, R. Hegde, R. M. Godbole, A. Grau, G. Pancheri, et al., Phys.Lett. **B659**, 137 (2008), arXiv:0708.3626 [hep-ph].
  - [3] A. Achilli, R. M. Godbole, A. Grau, G. Pancheri, O. Shekhovtsova, et al., Phys.Rev. **D84**, 094009 (2011), arXiv:1102.1949 [hep-ph].
  - [4] J. L. Rosner, Phys.Rev. **D90**, 117902 (2014), arXiv:1409.5813 [hep-ph].
  - [5] A. Grau, G. Pancheri, and Y. Srivastava, Phys.Rev. **D60**, 114020 (1999), arXiv:hep-ph/9905228 [hep-ph].
  - [6] E. Gotsman, E. Levin, and U. Maor, Phys.Lett. **B716**, 425 (2012), arXiv:1208.0898 [hep-ph].
  - [7] V. Khoze, A. Martin, and M. Ryskin, J.Phys. **G42**, 025003 (2015), arXiv:1410.0508 [hep-ph].
  - [8] M. Gluck, E. Reya, and A. Vogt, Z. Phys. **C53**, 127 (1992).
  - [9] M. Gluck, E. Reya, and A. Vogt, Z. Phys. **C67**, 433 (1995).
  - [10] M. Gluck, E. Reya, and A. Vogt, Eur. Phys. J. **C5**, 461 (1998), arXiv:hep-ph/9806404.
  - [11] A. D. Martin, R. G. Roberts, W. J. Stirling, and R. S. Thorne, Eur. Phys. J. **C4**, 463 (1998), arXiv:hep-ph/9803445.
  - [12] A. Martin, W. Stirling, R. Thorne, and G. Watt, Eur.Phys.J. **C63**, 189 (2009), arXiv:0901.0002 [hep-ph].
  - [13] R. M. Godbole, A. Grau, G. Pancheri, and Y. N. Srivastava, Phys. Rev. **D72**, 076001 (2005), arXiv:hep-ph/0408355.
  - [14] A. Corsetti, A. Grau, G. Pancheri, and Y. N. Srivastava, Phys. Lett. **B382**, 282 (1996), arXiv:hep-ph/9605314.
  - [15] Y. L. Dokshitzer, D. Diakonov, and S. I. Troian, Phys. Lett. **B79**, 269 (1978).
  - [16] G. Parisi and R. Petronzio, Nucl. Phys. **B154**, 427 (1979).
  - [17] F. Bloch and A. Nordsieck, Phys. Rev. **52**, 54 (1937).
  - [18] A. Grau, R. M. Godbole, G. Pancheri, and Y. N. Srivastava, Phys.Lett. **B682**, 55 (2009), arXiv:0908.1426 [hep-ph].
  - [19] P. Chiappetta and M. Greco, Phys. Lett. **B106**, 219 (1981).
  - [20] G. Pancheri and Y. Srivastava, Phys.Lett. **B159**, 69 (1985).
  - [21] T. K. Gaisser and F. Halzen, Phys. Rev. Lett. **54**, 1754 (1985).
  - [22] L. Durand and H. Pi, Phys. Rev. **D40**, 1436 (1989).
  - [23] V. Khoze, A. Martin, and M. Ryskin, Eur.Phys.J. **C74**, 2756 (2014), arXiv:1312.3851 [hep-ph].
  - [24] M. Good and W. Walker, Phys.Rev. **120**, 1857 (1960).
  - [25] P. Lipari and M. Lusignoli, Phys. Rev. **D80**, 074014 (2009), arXiv:0908.0495 [hep-ph].
  - [26] P. Lipari and M. Lusignoli, Eur.Phys.J. **C73**, 2630 (2013), arXiv:1305.7216 [hep-ph].
  - [27] M. Ryskin, A. Martin, and V. Khoze, Eur.Phys.J. **C72**, 1937 (2012), arXiv:1201.6298 [hep-ph].
  - [28] E. Gotsman, E. Levin, and U. Maor, Phys.Rev. **D85**, 094007 (2012), arXiv:1203.2419 [hep-ph].
  - [29] S. Ostapchenko, Phys.Rev. **D83**, 014018 (2011), arXiv:1010.1869 [hep-ph].
  - [30] I. Balitsky, Nucl.Phys. **B463**, 99 (1996), arXiv:hep-ph/9509348 [hep-ph].
  - [31] Y. V. Kovchegov, Phys.Rev. **D64**, 114016 (2001), arXiv:hep-ph/0107256 [hep-ph].
  - [32] S. Ostapchenko, Phys.Rev. **D81**, 114028 (2010), arXiv:1003.0196 [hep-ph].
  - [33] A. Grau, G. Pancheri, O. Shekhovtsova, and Y. N. Srivastava, Phys.Lett. **B693**, 456 (2010), arXiv:1008.4119 [hep-ph].
  - [34] G. Antchev et al. (TOTEM Collaboration), Phys.Rev.Lett. **111**, 012001 (2013).
  - [35] G. Antchev et al. (TOTEM), Europhys.Lett. **101**, 21004 (2013).
  - [36] G. Aad et al. (ATLAS), Nucl.Phys. **B889**, 486 (2014), arXiv:1408.5778 [hep-ex].
  - [37] M. M. Block and F. Halzen, Phys.Rev.Lett. **107**, 212002 (2011), arXiv:1109.2041 [hep-ph].
  - [38] D. A. Fagundes, M. J. Menon, and P. V. R. G. Silva, J.Phys. **G40**, 065005 (2013), arXiv:1208.3456 [hep-ph].
  - [39] D. A. Fagundes, A. Grau, G. Pancheri, Y. N. Srivastava, and O. Shekhovtsova, EPJ Web Conf. **90**, 03002 (2015), arXiv:1408.2921 [hep-ph].
  - [40] A. Giannini and F. Duraes, Phys.Rev. **D88**, 114004 (2013), arXiv:1302.3765 [hep-ph].
  - [41] G. Aad et al. (ATLAS Collaboration), Nature Commun. **2**, 463 (2011), arXiv:1104.0326 [hep-ex].

- [42] S. Chatrchyan et al. (CMS Collaboration), Phys.Lett. **B722**, 5 (2013), arXiv:1210.6718 [hep-ex].
- [43] G. Antchev et al. (TOTEM), Europhys.Lett. **101**, 21003 (2013).
- [44] B. Abelev et al. (ALICE Collaboration), Eur.Phys.J. **C73**, 2456 (2013), arXiv:1208.4968 [hep-ex].
- [45] R. Aaij et al. (LHCb), JHEP **1502**, 129 (2015), arXiv:1412.2500 [hep-ex].
- [46] S. Ostapchenko, Phys.Rev. **D89**, 074009 (2014), arXiv:1402.5084 [hep-ph].
- [47] S. Ostapchenko, Phys.Rev. **D74**, 014026 (2006), arXiv:hep-ph/0505259 [hep-ph].
- [48] A. K. Kohara, E. Ferreira, and T. Kodama, J.Phys. **G41**, 115003 (2014), arXiv:1406.5773 [hep-ph].
- [49] K. Goulianos, EPJ Web Conf. **71**, 00050 (2014).
- [50] P. Abreu et al. (Pierre Auger Collaboration), Phys.Rev.Lett. **109**, 062002 (2012), arXiv:1208.1520 [hep-ex].
- [51] M. M. Block and F. Halzen, Phys.Rev. **D83**, 077901 (2011), arXiv:1102.3163 [hep-ph].
- [52] D. A. Fagundes, A. Grau, S. Pacetti, G. Pancheri, and Y. N. Srivastava, Phys.Rev. **D88**, 094019 (2013), arXiv:1306.0452 [hep-ph].
- [53] R. Phillips and V. D. Barger, Phys.Lett. **B46**, 412 (1973).
- [54] N. A. Amos et al. (E710 Collaboration), Phys.Lett. **B301**, 313 (1993).
- [55] R. Ansorge et al. (UA5 Collaboration), Z.Phys. **C33**, 175 (1986).
- [56] G. Alner et al. (UA5 Collaboration), Phys.Rept. **154**, 247 (1987).
- [57] D. Bernard et al. (UA4 Collaboration), Phys.Lett. **B186**, 227 (1987).
- [58] J. Armitage, P. Benz, G. Bobbink, F. Erne, P. Kooijman, et al., Nucl.Phys. **B194**, 365 (1982).
- [59] T. Affolder et al. (CDF Collaboration), Phys.Rev.Lett. **87**, 141802 (2001), arXiv:hep-ex/0107070 [hep-ex].
- [60] D. Dutta (on behalf of CMS Collaboration), (2014), arXiv:1412.4977 [hep-ex].
- [61] R. Engel and R. Ulrich, Internal Pierre Auger Note **GAP-2012** (March, 2012).
- [62] G. Antchev et al. (TOTEM Collaboration), Phys.Rev.Lett. **111**, 262001 (2013), arXiv:1308.6722 [hep-ex].
- [63] B. Kopeliovich, Phys.Rev. **C68**, 044906 (2003), arXiv:nucl-th/0306044 [nucl-th].